# Water Adsorption and Hydrothermal Stability of CHA Zeolites with Different Si/Al Ratios and Compensating Cations

Moura, P.A.S.[1*], Rodríguez-Aguado, E.[2], Maia, D.A.S.[1], Melo, D.C.[3], Singh, R.[4], Valencia, S.[5], Webley P.A.[6], Rey, F.[5], Bastos-Neto, M.[1], Rodríguez-Castellón, E.[2], Azevedo, D.C.S.[1*]

[1] Grupo de Pesquisa em Separações por Adsorção, Federal University of Ceará, Fortaleza 60440-900, Brazil

[2] Departamento de Química Inorgánica, Facultad de Ciencias, University of Málaga, Málaga 29071, Spain

[3] CENPES/Petrobras, Rio de Janeiro, Brazil

[4] Clean Energy Laboratory, University of Melbourne, Melbourne 3010, Australia

[5] Instituto de Tecnología Química, Consejo Superior de Investigaciones Científicas – Universitat Politècnica de València Valencia 46022, Spain

[6] Department of Chemical Engineering, Monash University, Melbourne 3800, Australia

* Corresponding authors

Abstract

Zeolites are well known crystalline aluminosilicates, which may be used in processes that take advantage of their molecular sieving effect, such as natural gas drying. They are often used in cyclic processes that swing pressure and/or temperature to perform adsorption and desorption steps. It is recognized that thermal stress may decrease process performance upon prolonged use. In this work, chabazite (CHA) zeolite with two different Si/Al ratios and compensating cations was investigated by thermally aging the samples using a laboratory-scale protocol. A Premature Aging Protocol – PAP was proposed that took into account the conditions which the adsorbent is exposed to in Temperature Swing Adsorption (TSA) process for natural gas drying. The sample was previously saturated with water and *n*-heptane vapors (as a reference hydrocarbon) followed by pressurization (30 bar) and heating (573 K) with a mixture of $CO_2$ and $CH_4$ (1:4, v/v). The Si/Al ratios of the CHA samples under study were 2 and 5 and the compensating cations were *Na* and *K*. Aged materials presented a lower $CO_2$ and water vapor adsorption capacity with an increasing content of carbon in the bulk composition. The sample with higher Si/Al ratio (≈5) had a larger pore volume but adsorbed less water. Despite having the highest carbon content after aging and modest acidity, it was the most thermally stable sample, together with the sample containing potassium. Even with a lower Si/Al ratio (≈2), the presence of potassium provided the sample a protective effect against aging.

Keywords: molecular sieves, CHA, hydrothermal aging, water adsorption, Si/Al

## 1. Introduction

Zeolites are one of the most commonly employed adsorbents in drying TSA processes [1,2]. Some of the features that justify their widespread use in adsorption processes are high porosity, tunable acidity, high affinity for water at low partial pressures and good thermal stability. Most of these features are related to the *Al* content (**Figure 1**) and the nature of the cation (or proton) required to neutralize the negative framework charge. The amount of *Al* in zeolites is limited by the Löewenstein rule [3], that forbids – *Al* – *O* – *Al* – bonds. Aluminum atoms may be present in the zeolites, either as the tetrahedron $AlO_4$, which provides of negative charge, or as extra-framework octahedral *Al*. Even at room temperature, *Al* coordination may oscillate between tetrahedral and octahedral coordination [4]. The *Al* content in tetrahedral framework structures contributes to the material acidity by forming Brönsted sites. In zeolites, the Brönsted sites are composed by a proton ($H^+$), as compensating cation, linked to an oxygen atom that is part of – *Al* – *O* – *Si* – framework elements. As a result, these *O* atoms have a similar coordination as that found in hydronium cations ($H_3O^+$), giving rise to the well-known bridged hydroxyl or acid Brönsted sites in zeolites frameworks [5,6]. Bronsted acidity is mainly responsible for the catalytic activity of protonic zeolites. On the other hand, zeolites used as adsorbents have cations (alkali or earth alkali), instead of protons, to balance the negative charge brought about by the presence of *Al*. The presence of cations, typically *Na*, enhances the affinity for polar adsorbate molecules, such as water. The higher is the content of aluminum in the framework, the more cations are required to balance the charge and the higher water uptake is expected. Bronsted sites rarely occur in cationic zeolites, but Lewis acid sites

may occur due to structure defects or extra-framework (octahedral) aluminum [7].

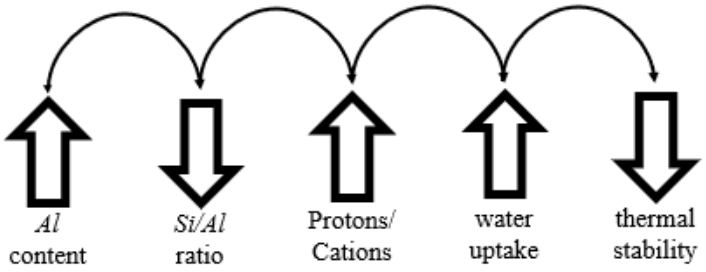


**Figure 1**. Interrelation of the main features in zeolites

The critical kinetic diameter of $H_2O$ molecules is 0.27 *nm*, thus cationic zeolites with small pores – such as CHA or LTA – have a high selectivity in drying processes. Besides their hydrophilic character, the choice of zeolites as drying agents also comes from their considerable thermal stability/resistance [8]. Generally speaking, the thermal resistance of zeolites is proportional to the Si content in the framework because *Si – O – Si* bonds are more thermally stable than *Si – O – Al* bonds, thus preventing disruption in crystallinity and porosity at high temperatures [9–11]. In addition, the possibility of cation exchange in Al-containing zeolites (to equilibrate the total charge) may modify its adsorption properties and thermal resistance. It has been reported that potassium cations lead to increased thermal stability [12], even though the larger ion size (e.g. as compared to $Na^+$) may also affect sorbate uptake. Chabazite (CHA) is a type of small pore zeolite (with a pore aperture of 0.38 *nm*) that may be synthesized in laboratory or found in naturally occurring deposits, in which case various cations are present. Chabazite has a framework

density of ≈14.5 T atoms (*Si* or *Al*) per nm³ [8], which is slightly higher than that of LTA, another commonly employed zeolite in gas drying. Regarding thermal resistance, *Cruciani* introduced a Stability Index in 2006 [9], which classified CHA with the highest score for thermal stability among several zeolites [13,14].

In offshore natural gas production facilities, gas drying by TSA is a mandatory unit operation, following the removal of condensates and particulate matter. In the adsorption step of a drying TSA cycle, the adsorbent packed in a column is ordinarily submitted to high pressures (around 30 bar) and a gas feed containing $CO_2$, $H_2O$ and trace heavier hydrocarbons (*C5+*), besides methane. After being loaded with water, the column is heated to desorb water and clean the adsorbent for another adsorption step. Even though the general correlations between zeolite features and its drying capacity and thermal stability are well known, the combined effect of water, traces of heavy hydrocarbons, high pressure and temperature in a confined pore, such as the small pore of CHA, is yet to be investigated. A better understanding about the interplay of zeolite characteristics (such as acidity, Si/Al, cations) and its thermal stability and water uptake under these severe conditions should help identify the causes of premature aging and guide the choice of robust and high-capacity adsorbents for TSA drying.

Therefore, the aim of this work is to investigate the influence of the *Si/Al* ratio and the compensating cation of CHA zeolites on their thermal stability and water uptake, considering process conditions currently found in offshore natural gas TSA drying. The materials stability was assessed by means of an aging protocol which accounted for the conditions found in TSA natural gas drying and the trade-off between the main adsorbent features that impact on the

material performance is analyzed. Three CHA zeolite samples were synthetized with different Si/Al ratios (approximately 2 and 5) in sodium and potassium forms. Then, the samples were submitted to a Premature Aging Protocol (PAP) that mimics the severity of TSA processes for natural gas drying. Before and after undergoing the PAP, samples were characterized by X-Ray Diffraction (XRD), X-Ray Photoelectron Spectroscopy (XPS), CHN Elemental Analysis and Inductively Coupled Plasma – Optical Emission Spectroscopy. $N_2$ adsorption/desorption isotherms at 77 K, $CO_2$ adsorption isotherms at 273 K and $H_2O$ adsorption isotherms at 313 K were carried out to highlight the implications of the *Si/Al* ratio and compensating cation on the CHA samples textural and adsorption properties.

## 2. Experimental

### 2.1 CHA Zeolite Syntheses

The synthesis of CHA (*Si/Al* ~ 2) in sodium form was carried out according to Gaffney and Coe [15] and Ranjeet and Webley [16]. Briefly, aluminum hydroxide was mixed to sodium hydroxide 97 %, potassium hydroxide 85 % and Tetramethylammonium hydroxide pentahydrate (TMA) 97 %. Then, the silica source (Ludox-LS-30, supplied by Aldrich) was added. The final synthesis gel had the following composition: 0.16 $(TMA)_2O$ : 6.67 $Na_2O$ : 2.2 $K_2O$ : 17.5 $SiO_2$ : $Al_2O_3$ : 276 $H_2O$. The synthesis gel was placed in a propylene bottle inside a preheated oven at 358.15 K for 4 hours to allow for crystallization. The solids were recovered by vacuum filtration.

The synthesis of CHA (*Si/Al* ~ 5) in sodium form [17] requires an Organic Structure Direct Agent – OSDA, NNN-trimethyl-1-adamantammonium (*TMAda*), which was synthesized in house. First, 29.6 g 1-Adamantamine and 64 g Potassium Carbonate were mixed in 320 mL Chloroform under magnetic agitation for 30 minutes. Then, 75 g Methyl Iodide were added dropwise to the mixture under agitation in an ice bath. Thereafter, the solution remained under agitation for 5 days at room temperature. The precipitated solids were recovered by vacuum filtration and washed with diethyl ether, followed by extraction with chloroform. After the production of TMAda, the CHA zeolite was synthesized as follows. First, 11.490 g sodium silicate solution, 0.900 g zeolite powder (CBV500, supplied by Zeolyst®) and 1.600 g *TMAda* were added to 22.800 g $H_2O$ in a plastic beaker. The final synthesis gel composition was 1.000 $SiO_2$ : 0.027 $Al_2O_3$ : 0.090 *TMAda* : 0.340 $Na_2O$ : 25.000 $H_2O$. Then, the solution was stirred by mechanical agitation for 2 hours and transferred to two teflon-lined autoclaves. The autoclaves were placed in an oven for 5 days (at 408.15 K) to allow for crystallization. The precipitated solids were recovered by vacuum filtration. After the synthesis procedure described above, the sample underwent a calcination step at 823 K in air for 3 hours, in order to remove the remaining SDA. Samples were heated up to 623 K in a ramp of 2.2 °C $min^{-1}$ and they were kept for two hours at this temperature. Then, they were further heated up to 823 K at a heating rate of 1.3 °C $min^{-1}$ and for 3 hours.

The synthesis of CHA (*Si/Al* ~ 2) in potassium form was based on Bourgogne et al. [18]. Briefly, 1.420 g *KOH* were dissolved in 21.300 g $H_2O$ in a polypropylene bottle. Then, 2.500 g zeolite Y powder (CBV500, supplied by Zeolyst) were added to the solution and stirred for 30 minutes. The final

synthesis gel composition was 0.170 $Na_2O$ : 2.000 $K_2O$ : 1.000 $Al_2O_3$ : 5.180 $SiO_2$ : 224.000 $H_2O$. Thereafter, the solution stood in an oven for 2 days (at 373.15 K) to allow for crystallization. The precipitated solids were separated by vacuum filtration. **Table 1** summarizes all zeolite samples and their labels.

**Table 1**. Summary of the zeolite samples and their labels

| Label | Material Description |
|---|---|
| CHA-SiAl2-Na–(V or A30) | Chabazite crystals in sodium form, with a Si/Al ratio of approximately 2, pristine (V) sample or aged sample for 30 days (A30) |
| CHA-SiAl5-Na–(V or A30) | Chabazite crystals in sodium form, with a Si/Al ratio of approximately 5, pristine (V) sample or aged sample for 30 days (A30) |
| CHA-SiAl2-K–(V or A30) | Chabazite crystals in potassium form, with a Si/Al ratio of approximately 2, and pristine (V) sample or aged sample for 30 days (A30) |

## 2.2 Premature Aging Protocol

The Premature Aging Protocol (PAP) consisted in exposing the zeolite sample to the typical conditions found in temperature swing adsorption (TSA) natural gas drying (**Figure 2**), such as high pressures and temperatures combined with humidity, traces of hydrocarbons, $CH_4$ and $CO_2$. First, 1.0 g sample was placed in the port inside the aging chamber, which was degassed at $10^{-3}$ mbar for 1 hour. A stainless-steel cylinder (10 mL) was connected to the

aging chamber initially containing 1.0 mL *n*-heptane and 0.5 mL water per gram of sample. *n*-Heptane was chosen as a representative compound of the trace hydrocarbons (C5+) commonly present in offshore natural gas [19]. The amount of water was calculated from the typical water uptake in zeolites [20] plus the water vapor in equilibrium in the gas phase filling the cylinder, the chamber and the tubing in between. Then, the zeolite sample was saturated with water and n-heptane vapors by opening valve H and allowing 24 hours for equilibrium to be reached. Thereafter, valve H was closed and the aging chamber was pressurized up to 30 bar total pressure with a $CO_2/CH_4$ mixture (1:4 v/v). After 1 hour, valves D and E were closed and the temperature in the chamber was increased up to 573 K (5 K $min^{-1}$) by means of an electric resistance surrounding the chamber. The sample was left at his temperature (and final pressure 30 bar) for 30 days.

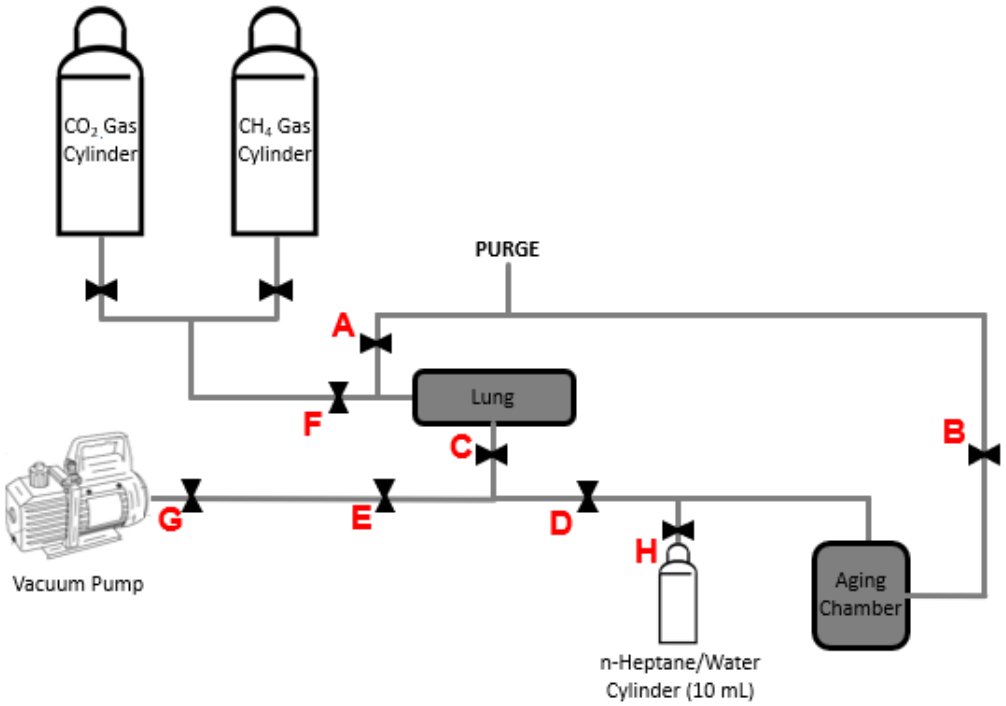

**Figure 2**. Premature Aging Protocol (PAP) scheme

## 2.3 Characterization Techniques and Adsorption Experiments

Zeolite samples were characterized before (V) and after being thermally aged for 30 days (A30) by XRD, XPS, ICP-OES and elemental analysis. XPS spectra were obtained in a Physical Electronic spectrometer (PHI Versa Probe II); X-Ray Diffraction patterns, in a X´Pert Pro MPD automated diffractometer (PANalytical®). Inductively Coupled Plasma – Orbital Emission Spectroscopy (ICP-OES) was carried out in an Agilent 715-ESTM instrument and Elemental Analysis CNH, in a Leco TruSpec Micro CHNSO elemental analyzer.

To measure the total acidity of the samples (pristine and aged materials), Temperature Programmed Desorption of $NH_3$ were performed. Briefly, 80 mg of an adsorbent sample were treated by flowing helium (100 mL $min^{-1}$) and heating from room temperature up to 620 °C at a rate of 3 °C $min^{-1}$. Then, ammonia diluted in He flows through the sample at 100 °C until complete saturation as detected by a mass spectrometer detector. Finally, ammonia is desorbed, by switching the flow to He and heating the sample from 100 to 800 °C at a rate of 10 ºC $min^{-1}$.

The porous texture of pristine (V) and aged (A30) samples was assessed by adsorption isotherms of probe gases $N_2$ (at 77 K) and $CO_2$ (at 273 K), which were measured in a Autosorb iQ3, by Quantachrome Instruments. Apparent BET surface areas and total pore volume were obtained from the $N_2$ isotherms [21] and the Dubinin-Radushkevich (DR) method was applied to estimate micropore volumes [22].

Water vapor adsorption isotherms were measured using a high-accuracy gravimetric instrument IGA-002, by Hiden® (UK) at 313 K and a pressure range up to 70 mbar. Prior to the experiments, samples were degassed at high vacuum ($10^{-5}$ mbar) and 573K for 10 hours. The experimental adsorption isotherm data was adjusted by the Aranovich-Donohue Model – ADM (**Eq. 01**) [23]. The ADM considers both "Langmuir type" behavior at low pressures combined with multi-layer adsorption (water clustering) and it has been already used to reproduce type II/IV water isotherms [24,25]. Thus, it is the product of two terms, the first one representing the Sips Model equation [26]. The second term accounts for the behavior at higher pressures and it considers the saturation pressure "$P_0$" and an empirical parameter "e" with no precise physical meaning. However, the magnitude of "e" is related to the relative importance of multilayer/clustering adsorption as compared to micropore filling.

$$q_{eq} = \frac{q_{máx} \cdot (b \cdot P)^n}{1 + (b \cdot P)^n} \cdot \frac{1}{1 - \left(\frac{P_o}{P}\right)^{\epsilon}} \qquad \textbf{Eq. 01}$$

## 3. Results and Discussion

The X-ray diffractograms of the pristine and aged samples are shown in **Figure 3**. The overall intensities of the diffraction peaks of the aged samples are lower, but the peak positions do not significantly change. Also, the absence of the typical broad band at 20 - 30 degrees characteristic of the presence of amorphous solid indicates that CHA samples do not undergo drastic

modifications upon aging. For all samples, irrespective the Si/Al ratio, the nature of the cation or the extent of aging (V or A30), the main characteristic diffraction peaks of a CHA structure are present and located in similar positions that those previously reported for CHA materials of similar Al contents [8].

**Table 2** summarizes the crystallinity of the aged samples, defined as the sum of areas under the main peaks in the range from 20 to 32° divided by the same sum for the pristine sample. As expected, a higher *Si/Al* ratio (5) for the Na samples leads to superior crystallinity, despite undergoing the aging protocol. The crystallinity of CHA sample with *Si/Al* ~ 2 (CHAc-SiAl2-Na-A30) decreases by 31% upon aging, whereas the sample with a higher Si/Al retains nearly the same crystallinity. The robustness of the latter sample is due to a superior thermal stability of *Si–O* bonds as compared to *Al–O* bonds, which means that more energy is required to break the former [9,10]. On the other hand, for the CHA samples with the same *Si/Al* ratio and different compensating cations, the presence of *K* renders the crystal lattice of CHA-type zeolites a higher resistance to aging. The presence of $K^+$ as compensating cations acts as a transformation inhibitor in the materials, increasing its resistance to elevated temperatures [12].

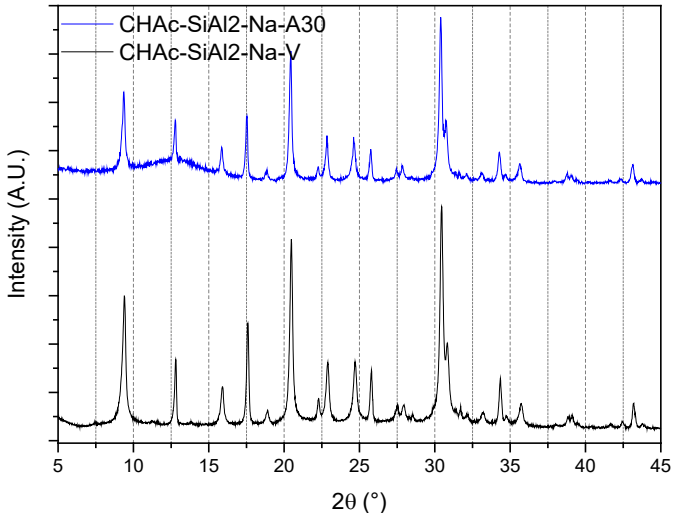


**(a)** CHAc-SiAl2-Na

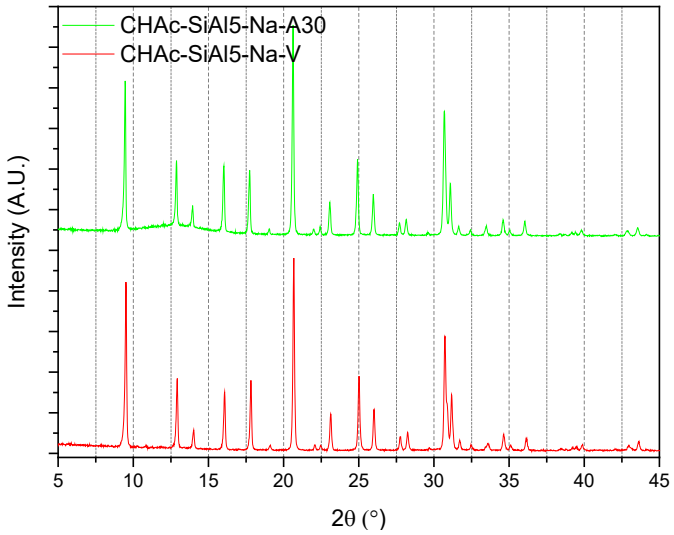


**(b)** CHAc-SiAl5-Na

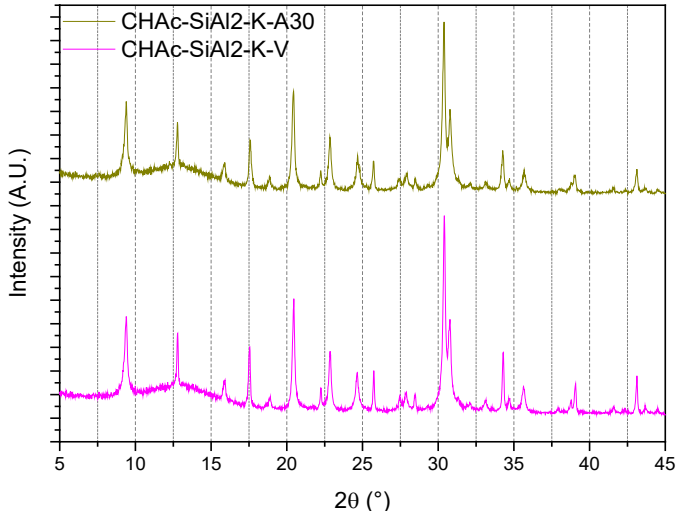


**(c)** CHAc-SiAl2-K

**Figure 3**. XRD diffractograms for the studied samples

**Table 2**. Materials crystallinity calculated from XRD diffractograms of the studied samples

| Sample | Crystallinity [%] |
|---|---|
| CHAc-SiAl2-Na-V | 100 |

| | |
|---|---|
| CHAc-SiAl2-Na-A30 | 68 |
| CHAc-SiAl5-Na-V | 100 |
| CHAc-SiAl5-Na-A30 | 96 |
| CHAc-SiAl2-K-V | 100 |
| CHAc-SiAl2-K-A30 | 90 |

The chemical surface composition, as determined by XPS for all samples under study, is shown in **Table 3**. The carbon content present on the surface of the pristine samples it is mostly attributed to adventitious carbon due to sample manipulation [27]. Except for the sample CHAc-SiAl2-K-V, all the other samples (Na form) display an increase in carbon content on the surface after undergoing the aging protocol, which may be related to coke formation [28]. This is likely to be related by the lower *Si/Al* and hence, increasing of acid sites, which may trigger more intense coke deposition and impact on the lower crystallinity, as observed in **Table 2**. For the same *Si/Al* ratio, the sample CHAc-SiAl2-K-V shows a lower carbon content on the surface after undergoing the aging protocol, which is an unexpected result. Because XPS is a spectroscopic technique that only examines the external surface, another technique to assess the chemical composition in the bulk may be useful to better understand this behavior. **Table 4** summarizes the binding energies found in the detailed spectral regions (not shown) of each of the identified elements in the samples. The Binding Energy (BE) for carbon (C 1*s*) accounts not only for bonds C – C (~284.6 eV), but also a small contribution from C – O (~286.3 eV); the binding energies for Si 2*p* (~102.5 eV) and Al 2*p* (~74.1 eV) are typical of the tetrahedral coordination in aluminosilicates and the binding energy for O 1*s*

(~532.0 eV) also refers to aluminosilicates [29,30]. Note that *Al* is only present with a single binding energy and no octahedral coordination (extra-framework *Al*) was detected on the surface of either the pristine or aged samples. The theoretical *Si/Al* ratios of the samples approximately match those found by XPS in the case of *Si/Al*=2 (**Table 5**). For the sample CHAc-SiAl5-Na-V, the *Si/Al* ratio on the surface is considerably higher than the theoretical value expected from the synthesis-gel composition (≈5), which suggests that *Al* atoms tend to be located in the bulk of the solid, rather than on the surface. Interestingly, the aging protocol led to an increase in the *Si/Al* ratio on the surface of all samples – a more pronounced behavior being observed for the samples with lower Si/Al in the pristine samples (**Table 5**). It may be postulated that, when the samples are aged, carbon deposits preferentially at the vicinity of Al-centered tetrahedra, due to its higher acidity as compared to Si-centered tetrahedra, thus covering the surface and causing a decrease in the Al atomic concentration (see **Table 3**).

**Table 3**. Chemical surface composition (% mass concentration) determined by XPS analysis for the studied samples

| Sample | C 1*s* | O 1*s* | Al 2*p* | Si 2*p* | Na 1*s* | K $2p_{3/2}$ |
|---|---|---|---|---|---|---|
| CHAc-SiAl2-Na-V | 17.8 | 59.0 | 5.5 | 11.9 | 5.2 | 0.6 |
| CHAc-SiAl2-Na-A30 | 23.5 | 55.0 | 4.1 | 10.2 | 6.8 | 0.5 |
| CHAc-SiAl5-Na-V | 18.6 | 62.5 | 1.9 | 14.2 | 2.8 | - |
| CHAc-SiAl5-Na-A30 | 22.1 | 59.8 | 1.7 | 14.0 | 2.5 | - |
| CHAc-SiAl2-K-V | 15.2 | 64.4 | 4.8 | 11.4 | - | 4.2 |
| CHAc-SiAl2-K-A30 | 12.1 | 66.6 | 4.6 | 12.6 | - | 4.1 |

**Table 4**. Binding Energy values (eV) and contributions for the studied samples

| Sample | Si 2*p* | Al 2*p* | C 1*s* | O 1*s* | Na 1*s* | K $2p_{3/2}$ |
|---|---|---|---|---|---|---|
| CHAc-SiAl2-Na-V | 102.6 | 74.6 | 285.0<br>286.6 | 531.8 | 1072.7 | 294.6 |
| CHAc-SiAl2-Na-A30 | 102.5 | 74.1 | 284.7<br>285.9 | 531.6 | 1072.3 | 294.5 |
| CHAc-SiAl5-Na-V | 103.1 | 74.3 | 284.8<br>286.3 | 532.5 | 1072.8 | - |
| CHAc-SiAl5-Na-A30 | 103.3 | 74.5 | 284.8<br>286.3 | 532.6 | 1073.0 | - |
| CHAc-SiAl2-K-V | 102.4 | 74.2 | 284.9<br>286.3 | 531.5 | - | 294.3 |
| CHAc-SiAl2-K-A30 | 102.5 | 74.1 | 284.7<br>286.0 | 531.6 | - | 294.3 |

**Table 5**. Obtained *Si/Al* atomic ratios determined by XPS analysis for the studied samples

| Sample | *Si/Al* atomic ratio |
|---|---|
| CHAc-SiAl2-Na-V | 2.24 |
| CHAc-SiAl2-Na-A30 | 2.60 (+13.8%) |
| CHAc-SiAl5-Na-V | 7.93 |
| CHAc-SiAl5-Na-A30 | 8.52 (+6.9%) |
| CHAc-SiAl2-K-V | 2.40 |
| CHAc-SiAl2-K-A30 | 2.85 (+12.2%) |

The chemical composition of the samples, as obtained from ICP-OES (**Table 6**), allows quantifying the elements in the solid bulk. Acceptable deviations from the theoretical Si/Al ratio are observed (less than 5% for the samples with lower Si/Al). By comparing the *Si/Al* ratios found by XPS and ICP-OES for sample CHAc-SiAl5-Na-V, it becomes evident that *A*l atoms tend to be located in the bulk of the solid and not on the surface in pristine materials. The content of elements *Na* and *K*, the compensating cations, is consistent with the composition of the respective synthesis gels mentioned in section 2.1. From the column (Na +K)/Al in the **Table 6**, it is possible to conclude that all the negative charge generated in the structure by the Al atoms is compensated by the sum of Na and K cations in the samples with Si/Al = 2, in which case the presence of Bronsted acid sites is ruled off. In the case of the sample CHAc-SiAl5-Na-V, there are more Al atoms than compensating cations available, which is likely to produce a negative charge that must be neutralized by protons, possible giving rise to Bronsted acid sites. On the other hand, this additional content of *Al* may be present as extra-framework *Al* may also be present as extra-framework Al or defective sites (Lewis acidity).

**Table 6**. ICP-OES from samples CHAc-SiAl(2, 5)–(Na, K)–V [*% Weight*]

| Sample | *Si* | *Al* | *Na* | *K* | *Si/Al* Ratio | *(Na + K)/Al* |
|---|---|---|---|---|---|---|
| CHAc-SiAl2-Na-V | 49.22 | 24.85 | 16.94 | 8.98 | 1.90 | 1.05 |
| CHAc-SiAl5-Na-V | 74.83 | 16.48 | 8.59 | 0.10 | 4.36 | 0.62* |
| CHAc-SiAl2-K-V | 46.87 | 21.51 | 0.07 | 31.56 | 2.09 | 1.01 |

The results of the elemental analysis are summarized in **Table 7** and, similarly to ICP-OES, they provide information on the carbon content in the bulk solid phase of the samples. For the samples with lower *Si/Al* ratio (CHAc-SiAl2-*Na* and CHAc-SiAl2-K), the increase in *C* content upon aging was modest as compared to that measured for the sample with higher *Si/Al* ratio (CHAc-SiAl5-Na). The content of *C* in the latter sample augmented, which is counterintuitive because a higher density of *Si – O – Si* bonds is expected to provide a more neutral framework with less coke deposition. The key role of acidity in the coke formation has been addressed by Guisnet at al. [28], who state that the strength of the acid sites in zeolites impact on the coke development. The acid sites in the inner porosity of zeolites catalyze the reactions of adsorbed hydrocarbons and the formed coke tends to build up in the pores [28]. On the other hand, the *C* content detected by *CNH* elemental analysis may not necessarily refer to coke, but physisorbed *n*-heptane if zeolite acidity is not strong enough to trigger coke formation. Considering XPS (**Table 3**) and CHN (**Table 7**), it is likely that the carbon deposition – whether as coke or as adsorbed hydrocarbons –occurs both in the outer surface and in the inner porosity in the case of the Na-loaded samples.

**Table 7**. CHN analysis for the studied samples

| Sample | *C content [%]* |
|---|---|
| | Measurement Uncertainty: ± 0.3 |
| CHAc-SiAl2-Na-V | 0.3 |

| | |
|---|---|
| CHAc-SiAl2-Na-A30 | 0.5 |
| CHAc-SiAl5-Na-V | 0.3 |
| CHAc-SiAl5-Na-A30 | 2.5 |
| CHAc-SiAl2-K-V | 0.3 |
| CHAc-SiAl2-K-A30 | 0.3 |

From the desorption profiles in Figure 4, it is possible to observe that most ammonia is physically adsorbed because desorption majorly takes place at a relatively mild temperature (below 300°C). This is especially true for the samples with Si/Al=2, which is consistent with the balance observed between (Na + K) and Al (**Table 6**), thus ruling off the presence of Bronsted acid sites in these samples. In the sample with Si/Al=2 containing Na, the deposition of carbon due to the aging protocol is therefore not due to Bronsted acid sites (BAS) in the fresh sample. Instead, BAS may be formed in the presence of water from Lewis sites in situ during the aging protocol, but this hypothesis requires further investigation. The sample showing the highest C deposition (CHAc-SiAl5-Na) (**Table 7**) was also the one with the highest amount of desorbed $NH_3$ at higher temperatures (above 300°C), suggesting the presence of Bronsted sites. This agrees well with the fact that there are more Al atoms than the sum of Na and K in this sample (**Table 6**). Interestingly, the aged sample (CHAc-SiAl5-Na-A30) is the one that undergoes the greatest reduction in desorbed $NH_3$ of all samples as compared to its fresh counterpart. This suggests that the carbon deposition brought about by aging may have partially deactivated the acid sites (those desorbing $NH_3$ above 300$^o$C) and considerably

reduced the available pore volume for ammonia adsorption (desorbed below 300ºC).

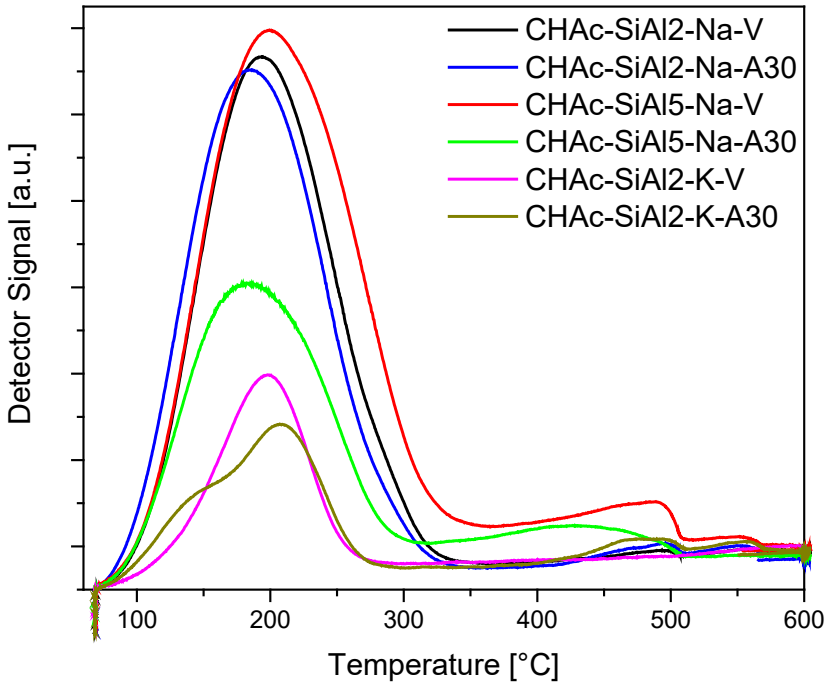


**Figure 4**. Detector signal in $NH_3$ temperature-programmed desorption for the studied samples

The $N_2$ isotherms at 77 K of the pristine and aged CHA samples are shown in **Figure 5**, Na containing samples featuring high uptakes at low relative pressures, a typical behavior of microporous solids [31]. Beyond relative pressure 0.8, all samples show a steep increase in $N_2$ uptake, which is likely to be due to condensation in interstitial voids between crystals. Analyzing the pristine samples with *Si/Al* ratios 2 and 5 in Na form, more adsorbed volume (and hence larger pore volume) is found for the sample CHAc-SiAl5-Na-V, which has less cations in the crystalline framework (see **Table 6**) thus allowing

for more N2 to be accommodated in the internal cages. A more drastic effect is observed when the samples with the same *Si/Al* and different compensation metals (*Na* and *K*) are compared. The adsorbed volume of $N_2$ in the plateau of the isotherm for the pristine Na sample is between 80 and 90 $cm^3\ g^{-1}$, whereas the pristine *K* sample adsorbs less than 20 $cm^3\ g^{-1}$. The critical kinetic diameter of cation $K^+$ is considerably larger than that of $Na^+$ [32], thus hindering the access of $N_2$ molecules to the cavities. As expected, the aged samples show a decrease in the adsorbed volume in nearly the whole relative pressure range, as compared to the pristine solids, although the isotherm shape remains about the same. The $N_2$ uptake reduction is more pronounced in the sample with the lower *Si/Al* ratio in Na form, which happens to be the one sample with the lower crystallinity and the largest build-up of carbon on the surface (see **Table 3**). Sample CHAc-SiAl5-Na-V, with the highest $N_2$ uptake, showed a less severe reduction, even though the bulk *C* content was the highest of all samples (**Table 7**) after aging, indicating that $N_2$ uptake is mostly dictated by the structural integrity of the zeolite.

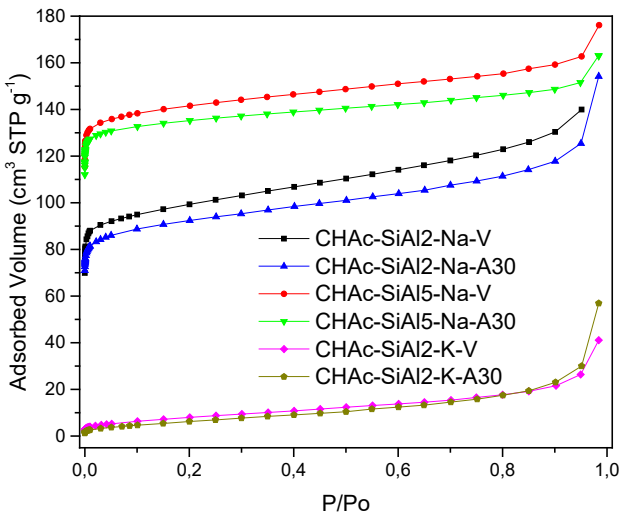


**(a)**

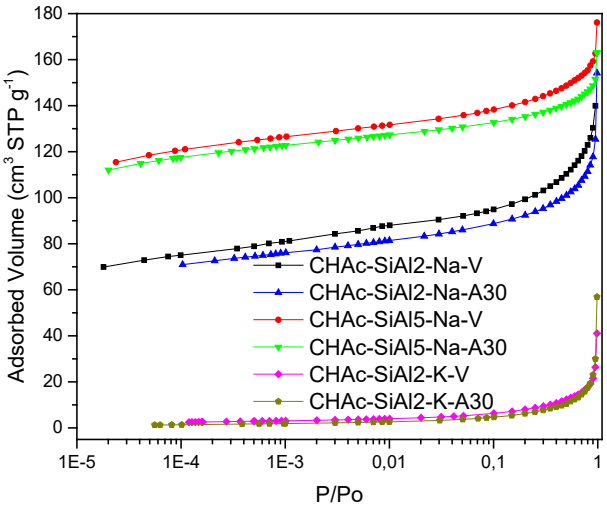


**(b)**

**Figure 5**. $N_2$ isotherms at 77 K for the studied samples in linear (a) and logarithmic (b) scales.

*$CO_2$* isotherms at 273 K for the samples under study are illustrated in **Figure 6**. Pore windows in some zeolites are so narrow that $N_2$ would diffuse through in an infinitely long time (e.g. LTA zeolites). The presence of voluminous cations may also lead to this behavior. Hence, the choice of *$CO_2$* as a probe gas stems from the fact that the analysis is carried out at a considerably higher temperature than $N_2$ and hence, very small cavities/pores may be accessed with a reasonable analysis time. From the isotherms (**Figure 6**), it is possible to see that a higher Si/Al ratio leads to a higher adsorption capacity for *$CO_2$*, like $N_2$, but only at sufficiently high relative pressures. At *$CO_2$* relative pressure below $10^{-3}$, the sample with a more polar surface (CHAc-SiAl2-Na) tends to retain more *$CO_2$*, due to a stronger adsorbent/adsorbate affinity. This affinity can also be explained by the high density of cations in the cage and the presence of both Na and K in significant amounts. It has been reported that $CO_2$ may interact with more than one cation by forming linearly bridged CO2 complexes on the dual-cation sites [33]. Beyond P/Po = $10^{-3}$, larger available pore space becomes the dominant factor that renders sample CHAc-SiAl5-Na the highest *$CO_2$* uptakes. Once again, the samples containing potassium have a smaller adsorption capacity and the isotherm is the least impacted due to hydrothermal aging. The results corroborate that the thermal resistance of these materials is closely related to the *Si/Al* ratio. As the *Si* content increases, the difference between the maximum *$CO_2$* uptake between the pristine and aged sample decreases. In fact, Cruciani [9] stated that zeolites with a Si/Al ratio higher than 3.80 are very stable upon heating.

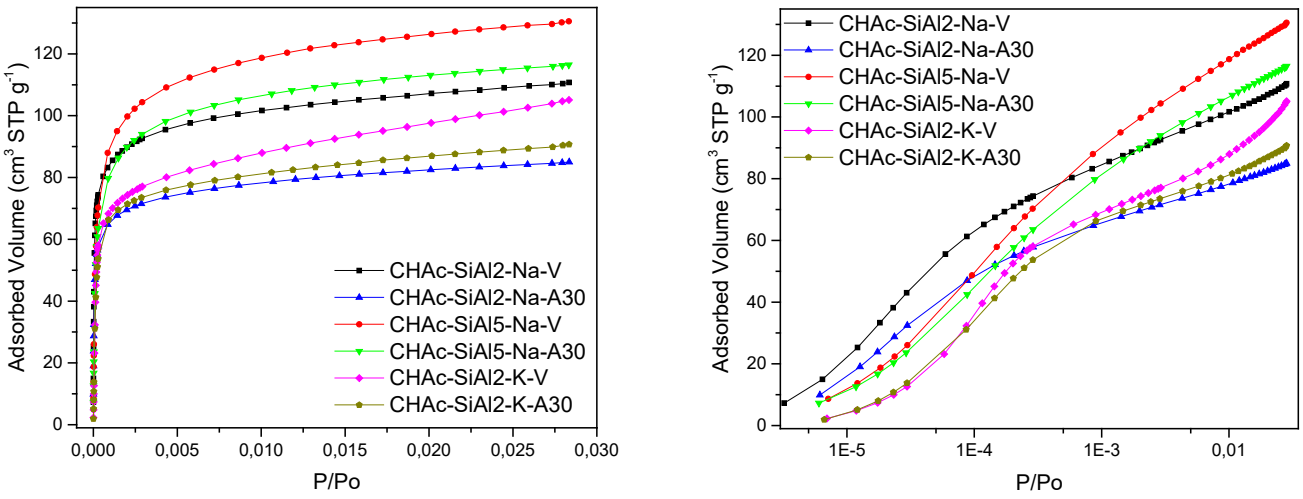


**Figure 6**. $CO_2$ adsorption isotherms at 273 K for the studied samples in linear (a) and logarithmic (b) scales.

On **Table 8**, important parameters to characterize the porous texture of the samples were determined from nitrogen and carbon dioxide adsorption isotherms at 77 and 273 K, respectively. The apparent (BET) specific surface area may be calculated from $N_2$ isotherms at 77 K and it has become a state-of-the-art methodology for porous solids [34]. Although not physically meaningful for microporous crystalline adsorbents, the BET area may be a useful figure of merit for the sake of comparison of the pore structure of samples. In addition, if the sample contains pore cavities into which $N_2$ adsorbs too slowly or does not adsorb at all, $CO_2$ adsorption isotherms at 273 K allow for a more precise calculation of the micropore volume [35]. The micropore volume of samples CHAc-SiAl2-Na, CHAc-SiAl5-Na, CHAc-SiAl2-K is reduced 22%, 11% and 8%, respectively, after undergoing the aging protocol. On one hand, the acidity brought about by the lower *Si/Al* content seems to lead to coke deposition, which obstructs the micropores to some extent (**Table 3** and **Table 8**) [28]. On

the other hand, even with a low *Si/Al*, the presence of *K* as compensating cation provides a protective effect against aging, also observed in Sun et al. [36]. This is likely to be due to a sieving effect that prevents the coke precursor (in this case, n-heptane) from accessing the internal cages, *i.e.*, the compensating cation acts as a shape-selective protection against coke deposition. The total porosity (from $N_2$ isotherms) for the pristine and aged samples with the highest Si/Al (**Table 8**) remains approximately the same, although it retains the largest amount of bulk carbon (**Table 7**) upon aging. If the carbon content in sample CHAc-SiAl5-Na-A30 refers to physiosorbed n-heptane, it is plausible that it is desorbed in the degassing steps prior to the isotherm measurements.

Water vapor adsorption isotherms were measured up to 70 mbar, which is close to the saturation pressure of water at 313 K (**Figure 7**). In the low-pressure zone (up to 10 mbar), there is a steep increase in uptake, indicating a high adsorbent-adsorbate interaction. A plateau on the adsorbed load is observed for all samples in the pressure range of 10 to 40 mbar. Zeolite CHAc-SiAl2-Na, both for the pristine and aged samples, shows a sharp increase at pressures beyond 40 mbar, which was less intense for the other four samples (CHAc-SiAl5-Na–(V, A30) and CHAc-SiAl2-K–(V, A30)) (**Figure 7**). The affinity of protonic zeolites for water molecules is mainly driven by the attraction between polar molecules (e.g. water) and the acid sites caused by unbalanced charges [37,38], as previously discussed. However, the compensating cations in cationic zeolites also attract water molecules, an example is the zeolite 3A typically applied in drying processes for organics [39]. The electronegativity in water molecules leads to positive and negative charges in *H* and *O*, respectively, and thus the *O* atom in water behaves as a Brönsted

basic site. On the other hand, the $AlO_4^-$ units that compose the zeolite framework act as a Bronsted acid site so that dipole-field interaction causes the retention of the water molecules in the zeolite cage [40]. Therefore, the *Al* content (and hence the *Si/Al* ratio) is a determining factor in water uptake both in cationic and protonic zeolites [9,41]. This explains why the sample CHAc-SiAl2-Na-V has a higher adsorption capacity for water than the sample CHAc-SiAl5-Na-V, as a result of the higher density of cations. In addition, by comparing the samples CHAc-SiAl2-Na-V and the CHAc-SiAl2-K-V, the larger size of potassium cation is reflected in a lower water uptake for the latter sample which has no Na cations.

**Table 8**. BET apparent surface area, pore volume, adsorption capacity and micropore volume for the for the studied samples

| Sample | from $N_2$ Isotherms at 77 K | | from $CO_2$ Isotherms at 273 K | |
|---|---|---|---|---|
| | Surface Area [$m^2\ g^{-1}$] | Total Pore Volume [$cm^3\ g^{-1}$] | Adsorption Capacity * [$cm^3\ g^{-1}$] | Micropore Volume [$cm^3\ g^{-1}$] |
| CHAc-SiAl2-Na-V | 308 | 0.281 | 110.7 | 0.225 |
| CHAc-SiAl2-Na-A30 | 267 | 0.164 | 85.0 | 0.174 |
| CHAc-SiAl5-Na-V | 444 | 0.233 | 130.5 | 0.282 |
| CHAc-SiAl5-Na-A30 | 392 | 0.227 | 116.4 | 0.251 |
| CHAc-SiAl2-K-V | 31 | 0.031 | 105.1 | 0.200 |
| CHAc-SiAl2-K-A30 | 13 | 0.013 | 90.7 | 0.184 |

* measured at a relative pressure of 0.029

References: [21,22]

By comparing pristine and respective aged materials, for *Na*-containing samples, a higher content of *Si* promotes greater hydrothermal stability [9], which is confirmed by the isotherms of samples with different Si/Al ratios. For the sample with *Si/Al* ratio of approximately 2, the maximum water vapor adsorption capacity decreases by 14% upon aging (**Table 9**) whereas it decreases by 10% for the sample with higher *Si/Al* ratio. This difference in stability is even more pronounced in the lower pressure range, as observed in the graph in logarithmic scale. Regarding the main compensation metal in the structure (*Na* and *K*), once again the presence of potassium seems to provide greater thermal stability, as observed in the water isotherms of the pristine and aged sample CHAc-SiAl2-K, particularly in the low-pressure range (**Figure 7b**). Note that the size of the compensating cation has a crucial contribution to the adsorption capacity, which is significantly lower for the sample containing *K* than for the sample containing *Na* in the whole pressure range and considering the same *Si/Al* ratio in both pristine samples. Given the robustness of the sample with lower *Si/Al* ratio containing potassium, it may be the adsorbent of choice for prolonged use in cyclic TSA gas drying, despite the significantly higher water uptake of the pristine *Na*-containing zeolite. This is more evident at low relative humidities of the gas phase (below 5 mbar), in which case the loss in water uptake is much more pronounced for the Na-sample (CHAc-SiAl2-Na). For humidity values close to the saturation point, the latter sample keeps a relatively high-water uptake, despite a partial deactivation (see **Table 9**).

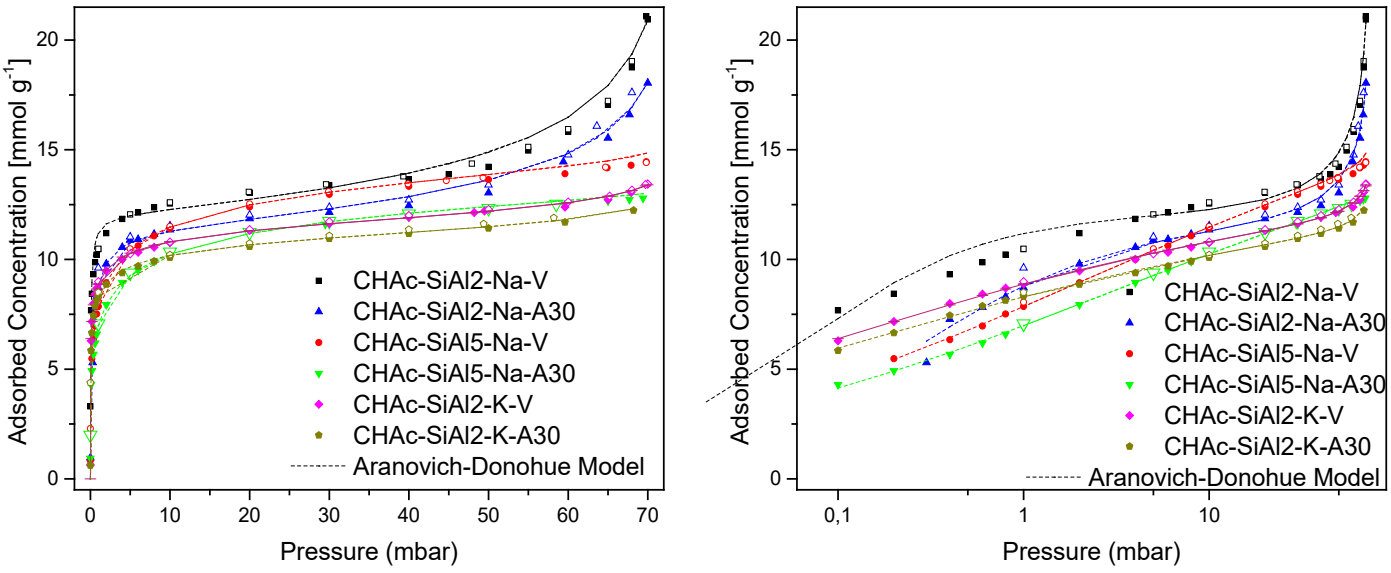


**Figure 7**. Water vapor adsorption Isotherms at 313 K for the studied samples in linear (a) and logarithmic (b) scales. Filled symbols: adsorption branch; Hollow symbols: desorption branch

**Table 9.** Water vapor capacity at 70 mbar and 313 K for the studied samples

| Sample | | Maximum $H_2O_{(v)}$ Adsorption Capacity [mmol $g^{-1}$] |
|---|---|---|
| CHAc-SiAl2-Na | V | 20.9 |
| | A30 | 18.0 |
| CHAc-SiAl5-Na | V | 14.5 |
| | A30 | 12.8 |
| CHAc-SiAl2-K | V | 13.4 |
| | A30 | 11.7 |

Experimental data from all isotherms were adequately fitted by the AD model with calculated parameters summarized in **Table 10**. The ($q_{max}$) parameter was the highest for the sample with a higher Si/Al ratio, less cations

and thus larger available micropore volume (**Table 8**). Parameter (*b*), which accounts for the adsorbent-adsorbate interaction, radically decreases when the Si/Al ratio increases, which is consistent with a less ionic framework. The parameter (*n*), which is qualitatively related to the homogeneity of the adsorbent surface, was reduced upon aging for all samples (**Table 10**). Unlike the Langmuir/Sips model, the AD model satisfactorily described the increase in uptake observed at pressures close to the water vapor saturation pressure, particularly for sample CHAc-SiAl2-Na (V and A30). Although parameter "e" has no precise physical meaning, it is an empirical constant associated to water clustering or condensation in larger pores or interstitial voids between the zeolite crystals, which seems to be the case for sample CHAc-SiAl2-Na.

**Table 10**. Parameters used in Aranovich-Donohue model fitting for water vapor isotherms at 313 K for the studied samples

| Sample | Parameters | | | |
|---|---|---|---|---|
| | $q_{max}$ [mg g$^{-1}$] | $b$ [mbar$^{-1}$] | $n$ | $e$ |
| CHAc-SiAl2-Na-V | 217.41 | 16.07 | 0.90 | 0.19 |
| CHAc-SiAl2-Na-A30 | 208.96 | 4.09 | 0.80 | 0.15 |
| CHAc-SiAl5-Na-V | 313.59 | 0.59 | 0.37 | 0.02 |
| CHAc-SiAl5-Na-A30 | 306.40 | 0.34 | 0.34 | 0.01 |
| CHAc-SiAl2-K-V | 233.45 | 9.25 | 0.35 | 0.05 |
| CHAc-SiAl2-K-A30 | 224.86 | 7.60 | 0.34 | 0.04 |

## Conclusions

Chabazite samples were synthesized under different *Si/Al* ratios containing two types of compensating cations in order to investigate the impact of these features in water uptake and their resistance to thermal aging. The aging protocol caused a mild degradation of the crystalline structure of the samples, which was much less severe for samples with higher *Si/Al* and and greater content of *K*. All aged materials showed worsened textural characteristics, which seemed directly correlated to the increase in *C* content in the bulk, particularly for the samples with lower *Si/Al* ratio. Interestingly, the aging protocol affected the sample with the highest *Si/Al* (5) to a lesser extent in terms of textural properties and water uptake in spite of having the highest *C* content in the bulk. Despite the low Al content, this sample exhibited higher acidity, which was suggested by the unbalance with cations and confirmed by NH3 TPD experiments. It may be postulated that the hydrocarbon present in the aging protocol (*n*-heptane) is adsorbed in the pores of the zeolite, given its larger micropore volume, but the framework acidity is not strong enough to trigger coke formation that would irreversibly block pores. The presence of potassium as compensating cation also has a great impact on the hydrothermal stability. Due to its larger size as compared to sodium, it is likely that only water molecules have access to the pores reversibly, and not the hydrocarbon present in the aging protocol. As a result, upon aging, it is the one sample with the lowest increase in *C* bulk content and less affected in textural properties and water uptake. Given these characteristics, for prolonged TSA operation, the sample with potassium may provide a better trade-off between thermal stability and water uptake, particularly to dry gases with low relative humidities.

*Acknowledgments*

The authors acknowledge financial support from Petrobras, CNPq and CAPES, particularly in the frame of project CAPES/Print 88887.311867/2018-00. E. Rodríguez-Aguado and E. Rodríguez-Castellón are thankful to project RTI2018-099668-BC22 of *Ministerio de Ciencia, Innovación y Universidades* and project UMA18-FEDERJA-126 of *Junta de Andalucía* and FEDER funds. The authors S. Valencia and F. Rey are thankful to the MCIU, AEI and FEDER for funding through the projects RTI2018-101784-B-I00 and SEV-2016-0683.

References

[1] A. Aleghafouri, M. Davoudi, Modeling and simulation of a pressure–temperature swing adsorption process for dehydration of natural gas, Adsorption. 24 (2018) 121–133. https://doi.org/10.1007/s10450-017-9924-z.

[2] E. Gabruś, J. Nastaj, P. Tabero, T. Aleksandrzak, Experimental studies on 3A and 4A zeolite molecular sieves regeneration in TSA process: Aliphatic alcohols dewatering–water desorption, Chem. Eng. J. 259 (2015) 232–242. https://doi.org/10.1016/j.cej.2014.07.108.

[3] W. Loewenstein, The distribution of aluminum in the tetrahedra of silicates and aluminates., Am. Mineral. 39 (1954) 92–96.

[4] B. Xu, F. Rotunno, S. Bordiga, R. Prins, J. Vanbokhoven, Reversibility of

structural collapse in zeolite Y: Alkane cracking and characterization, J. Catal. 241 (2006) 66–73. https://doi.org/10.1016/j.jcat.2006.04.009.

[5] M. Boronat, A. Corma, What Is Measured When Measuring Acidity in Zeolites with Probe, (2019). https://doi.org/10.1021/acscatal.8b04317.

[6] T.K. Phung, G. Busca, On the Lewis acidity of protonic zeolites, Appl. Catal. A Gen. 504 (2015) 151–157. https://doi.org/10.1016/j.apcata.2014.11.031.

[7] M. Ravi, V.L. Sushkevich, J.A. van Bokhoven, Towards a better understanding of Lewis acidic aluminium in zeolites, Nat. Mater. 19 (2020) 1047–1056. https://doi.org/10.1038/s41563-020-0751-3.

[8] S. Mintova, N. Barrier, Verified Syntheses of Zeolitic Materials, Third Ed., International Zeolite Association - IZA, Caen - FR, 2016.

[9] G. Cruciani, Zeolites upon heating: Factors governing their thermal stability and structural changes, J. Phys. Chem. Solids. 67 (2006) 1973–1994. https://doi.org/10.1016/j.jpcs.2006.05.057.

[10] G.T. Kerr, Intracrystalline rearrangement of constitutive water in hydrogen zeolite Y, J. Phys. Chem. 71 (1967) 4155–4156. https://doi.org/10.1021/j100871a079.

[11] S. Sircar, A. Myers, Chapter 22. Gas Separation by Zeolites, in: Handb. Zeolite Sci. Technol., Marcel Dekker, Inc., 2003: pp. 1–42. https://doi.org/10.1201/9780203911167.ch22.

[12] S. Cartlidge, E.B. Keller, W.M. Meier, Role of potassium in the thermal stability of CHA- and EAB-type zeolites, Zeolites. 4 (1984) 226–230.

https://doi.org/10.1016/0144-2449(84)90028-9.

[13] G. Cruciani, A. Gualtieri, Dehydration dynamics of analcime by in situ synchroton powder diffraction, Am. Mineral. 84 (1999) 112–119. https://doi.org/10.2138/am-1999-1-212.

[14] S.H. Shim, A. Navrotsky, T.R. Gaffney, J.E. Macdougall, Chabazite: Energetics of hydration, enthalpy of formation, and effect of cations on stability, Am. Mineral. 84 (1999) 1870–1882. https://doi.org/10.2138/am-1999-11-1214.

[15] T.R. Gaffney, C.G. Coe, Processfor the Preparation of an Improved Chabazite for the Purification of Bulk Gases, 5,026,532, 1991.

[16] R.K. Singh, P. Webley, Adsorption of N2, O2, and Ar in potassium chabazite, Adsorption. 11 (2005) 173–177. https://doi.org/10.1007/s10450-005-5918-3.

[17] S.I. Zones, Conversion of faujasites to high-silica chabazite SSZ-13 in the presence of N,N,N-trimethyl-1-adamantammonium iodide, J. Chem. Soc. Faraday Trans. 87 (1991) 3709–3716. https://doi.org/10.1039/FT9918703709.

[18] M. Bourgogne, J.-L. Guth, R. Wey, Process for the preparation of synthetic zeolites, and zeolites obtained by said process, 4,503,024, 1985. http://www.google.com/patents/US4503024.

[19] R. Gomes Santiago, B. Ferreira dos Santos, I. Gomes Lima, K. Oliveira Moura, D. Carrijo Melo, W. Mantovani Grava, M. Bastos-Neto, S.M. Pereira de Lucena, D. Cristina Silva de Azevedo, Investigation of

premature aging of zeolites used in the drying of gas streams, Chem. Eng. Commun. 206 (2019) 1378–1385. https://doi.org/10.1080/00986445.2018.1533468.

[20] Y. Wang, Measurements and Modeling of Water Adsorption Isotherms of Zeolite Linde-Type A Crystals, Ind. Eng. Chem. Res. 59 (2020) 8304–8314. https://doi.org/10.1021/acs.iecr.9b06891.

[21] S. Brunauer, P.H. Emmett, E. Teller, Adsorption of Gases in Multimolecular Layers, J. Am. Chem. Soc. 60 (1938) 309–319. https://doi.org/10.1021/ja01269a023.

[22] L.V. Dubinin, M.M., Radushkevich, Equation of the characteristic curve of activated charcoal, Proc. Acad. Sci. Phys. Chem. Sec. USSR. 55 (1947) 331–333.

[23] G.L. Aranovich, M.D. Donohue, A New Approach to Analysis of Multilayer Adsorption, J. Colloid Interface Sci. 173 (1995) 515–520. https://doi.org/10.1006/jcis.1995.1353.

[24] J. Cieśla, Z. Sokołowska, B. Witkowska-Walczak, K. Skic, Adsorption of water vapour and the specific surface area of arctic zone soils (Spitsbergen), Int. Agrophysics. 32 (2018) 19–27. https://doi.org/10.1515/intag-2016-0076.

[25] H.-T. Oh, S.-J. Lim, J.H. Kim, C.-H. Lee, Adsorption Equilibria of Water Vapor on an Alumina/Zeolite 13X Composite and Silica Gel, J. Chem. Eng. Data. 62 (2017) 804–811. https://doi.org/10.1021/acs.jced.6b00850.

[26] a L. Myers, J.M. Prausnitz, Thermodynamics of mixed-gas adsorption,

AIChE J. 11 (1965) 121–127. https://doi.org/10.1002/aic.690110125.

[27] S. Evans, Correction for the effects of adventitious carbon overlayers in quantitative XPS analysis, Surf. Interface Anal. 25 (1997) 924–930. https://doi.org/10.1002/(SICI)1096-9918(199711)25:12<924::AID-SIA317>3.0.CO;2-2.

[28] M. Guisnet, P. Magnoux, D. Martin, Roles of acidity and pore structure in the deactivation of zeolites by carbonaceous deposits, in: 1997: pp. 1–19. https://doi.org/10.1016/S0167-2991(97)80138-3.

[29] G.E.M. C.D. Wagner, W.M. Riggs, L.E. Davis, J.F. Moulder, Handbook of X-Ray Photoelectron Spectroscopy, Perkin-Elmer Corporation, Physical Eletronics Division, Eden Prairie, Minnesota, 1979.

[30] S.R. Bare, A. Knop-Gericke, D. Teschner, M. Hävacker, R. Blume, T. Rocha, R. Schlögl, A.S.Y. Chan, N. Blackwell, M.E. Charochak, R. ter Veen, H.H. Brongersma, Surface analysis of zeolites: An XPS, variable kinetic energy XPS, and low energy ion scattering study, Surf. Sci. 648 (2016) 376–382. https://doi.org/10.1016/j.susc.2015.10.048.

[31] J. Silvestre-Albero, A. Silvestre-Albero, F. Rodríguez-Reinoso, M. Thommes, Physical characterization of activated carbons with narrow microporosity by nitrogen (77.4 K), carbon dioxide (273 K) and argon (87.3 K) adsorption in combination with immersion calorimetry, Carbon N. Y. 50 (2012) 3128–3133. https://doi.org/10.1016/j.carbon.2011.09.005.

[32] M.W.B. Theodore L., L. H. Eugene Jr., B. Bruce E., M. Catherine J., W. Patrick M., Stoltzfus, Chemsitry The Central Science, 14th Editi, 2017.

[33] A. Pulido, P. Nachtigall, A. Zukal, I. Dominguez, J. Čejka, Adsorption of CO 2 on sodium-exchanged ferrierites: The bridged CO 2 complexes formed between two extraframework cations, J. Phys. Chem. C. 113 (2009) 2928–2935. https://doi.org/10.1021/jp810038b.

[34] G. Rouquerol, F., Rouquerol, J., Sing, K., Llewellyn, P., Maurin, Adsorption at the Liquid-Solid Interface: Thermodynamics and Methodology., 2014. https://doi.org/10.1016/B978-0-08-097035-6.00004-8.

[35] J. García-Martínez, D. Cazorla-Amorós, A. Linares-Solano, Further evidences of the usefulness of CO2 adsorption to characterize microporous solids., in: Encycl. Volcanoes., 2000: pp. 485–494. https://doi.org/10.1016/S0167-2991(00)80054-3.

[36] P. Sun, D. Yu, K. Fu, M. Gu, Y. Wang, H. Huang, H. Ying, Potassium modified NaY: A selective and durable catalyst for dehydration of lactic acid to acrylic acid, Catal. Commun. 10 (2009) 1345–1349. https://doi.org/10.1016/j.catcom.2009.02.019.

[37] B.E. Poling, J.M. Prausnitz, J.P. O'Connell, The Properties of Gases and Liquids, Fifth Edit, McGRAW-HILL, New York, 2001. https://doi.org/10.1036/0070116822.

[38] A. Louis Allred, Electronegativity values from thermochemical data, J. Inorg. Nucl. Chem. 17 (1961) 215–221. https://doi.org/10.1021/jp020500+.

[39] A. Cadiau, Y. Belmabkhout, K. Adil, P.M. Bhatt, R.S. Pillai, A. Shkurenko, C. Martineau-Corcos, G. Maurin, M. Eddaoudi, Hydrolytically stable

fluorinated metal-organic frameworks for energy-efficient dehydration, Science (80-. ). 356 (2017) 731–735. https://doi.org/10.1126/science.aam8310.

[40] T. Kawai, K. Tsutsumi, Evaluation of hydrophilic-hydrophobic character of zeolites by measurements of their immersional heats in water, Colloid Polym. Sci. 270 (1992) 711–715. https://doi.org/10.1007/BF00654048.

[41] A. Corma, A. Martinez, Zeolites and Zeotypes as catalysts, Adv. Mater. 7 (1995) 137–144. https://doi.org/10.1002/adma.19950070206.